CONF-9510195--4
SAND95-2271C

CHARACTERIZATION OF A RESONANT PLATE SHOCK SYSTEM USING FINITE ELEMENT ANALYSIS

Dr. G. D. Gute
University of Missouri
5605 Troost Ave.
Kansas City, Missouri 64110
(816) 235-1284

D. G. Moore
Sandia National Laboratories
P.O. Box 5800-0615
Albuquerque, New Mexico 87185
(505) 844-7095

The dynamic performance of a 250 Hz resonant plate shock system which simulates pyrotechnic shock environments on micro-electrical components is evaluated. A series of experiments recording strain rate histories and acceleration time histories at several plate locations were conducted. This empirical data is used to compare the analytical results obtained from a finite element based numerical simulation. The comparison revealed a good correlation between experimental and analytical results.

INTRODUCTION

Resonant plate shock testing plays an important role in environmental testing of electrical and mechanical components by simulating pyrotechnic shock events detected in aerospace structures. This testing ensures that components purchased or manufactured by industry can remain operational and retain their structural integrity throughout their anticipated lives. Resonant plate shock testing has evolved from early work of Bai and Thatcher [1]. Bai and Thatcher developed a metal-to-metal impact machine. This machine produced a simulated pyrotechnic shock event by allowing a steel hammer to impact an aluminum beam. The event produced a very high g-shock that excited the dominant frequency of the test fixture. This frequency matched the fundamental frequency of the aluminum beam. Further work from Davie [2] controlled the response of the resonating beam by clamping mass to it. Davie concluded that the beam response can be controlled with additional mass clamped at node points. Bell and Zimmerman [3] studied pyrotechnic shock simulation by evaluating the test component attachment effects. Bell and Zimmerman concluded that dynamic interaction of the test assembly and a 1500 Hz plate is minimal. Bell and Pott [4] then studied the effects of damping systems on a 1300 Hz plate. Bell and Pott concluded that additional mass at appropriate locations on the plate edge provide the required damping characteristics without dramatically changing the frequency content of the plate. Bell and Pott also determined that the use of C-Clamps to attach the bars to the plate adds mechanical damping to a 1300 Hz plate but changes the plate frequency.

This paper is an in-depth study of a low frequency (250 Hz) resonate plate test assembly which simulates pyrotechnic shock events. The test assembly consists of a swing arm, test fixture, C-Clamps and a plate. The dynamic interaction of the plate using finite element analysis will also be examined. Collected empirical data verifies the finite element model.

This work was supported by the United States Department of Energy under Contract DE-AC04-94AL85000.

DISCLAIMER

THEORY OF FLAT PLATES

The plate examined for this study falls in the category of a thin plate thickness with small strains and large deflections. The plate notation is consistent with the foundation work of Timoshenko [5]. The x and y axes are at the undeformed middle surface of the plate with thickness of h and the incremental dimensions of dx and dy. This middle surface is called the neutral axis. When a load q acting over an area dxdy is applied, the plate deforms. The deformed middle surface of the plate element is expressed with the changes of the slope (Fig 1). The origin is placed at the middle of the element and displacement in the z-direction is w. When small strains are considered, summing forces in the z-direction yield equations developed by Leissa [6]. The equation is greatly reduced by expanding the terms with products, removing third-ordered differential terms and dividing through by the area. If in-plane inertia forces within the plate are neglected and transverse shearing stresses are small relative to the in-plane stresses, the equation can be reduced to the following form:

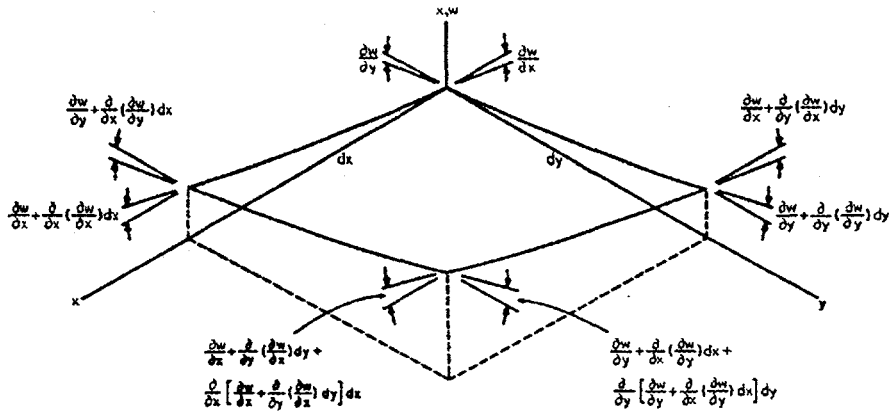

Figure 1. Deformed middle of the plate after a load is applied.

$$\frac{\partial Q_x}{\partial x}+\frac{\partial Q_y}{\partial y}+N_x\frac{\partial^2 w}{\partial x^2}+N_y\frac{\partial^2 w}{\partial y^2}+2N_{xy}\frac{\partial^2 w}{\partial x\partial y}+q=\rho\frac{\partial^2 w}{\partial t^2} \quad (1)$$ where:

Q_X = the transverse shearing force on the x surface.

Q_y = the transverse shearing force on the y surface.

q = the external load acting over the plate area $dxdy$

ρ = the mass density per unit area

$\frac{\partial^2 w}{\partial t^2}$ = the acceleration in the z-direction

N_X = the in-plane normal force on the cross sectional face of the element on the x axis per unit length of the y coordinate line.

N_y = the in-plane normal force on the cross sectional face of the element on the y axis per unit length of the x coordinate line.

N_{xy} = the shearing force on the x axis cross section in the y axis direction.

TEST APPARATUS

The airgun consists of an electrical pneumatic control system and a six foot long guide-tube that fires the projectile (Fig. 2). The projectile upon impact produces a high level pyrotechnic shock event which simulates structural responses found in aerospace systems. This type of shock pulse is characterized by an oscillatory acceleration-time history reaching several thousand g's and lasting from 5 -15 milliseconds. Pyrotechnic shock events have both positive and negative acceleration peaks with little or no velocity change. The exhaust slots in the guide-tube prevent the projectile from re-impacting the plate. The plate is held to the support frame in a pendulum fashion by a clevis. The rotational motion of the plate after impact is stopped by an electrical brake system. A projectile is loaded into the muzzle and fired at the plate. The air gun fires a 3-inch diameter forty pound projectile into a 26 x 26 x 0.75 inch 6061-T6 aluminum tooling plate. The plate responds at its predetermined natural frequency and produces oscillatory acceleration-time wave forms. The plate response is transmitted to the test fixture and the electrical component assembly.

Eight EA-06-500UV-120 type gages are installed on the plate at a radius of 9 inches from the center using M-Bond 610 adhesive (Fig.3). Strain gage measurements are taken in the x and y axis and in the xy plane. The strain gages are calibrated using quarter bridge completion circuits with a 10 volt excitation and shunt calibrated for 400 microinch full scale response. Four Endevco Model 2255B-025 accelerometers are bonded to the plate. The accelerometers measured acceleration time histories at three plate locations and one fixture location. The test objective is to determine what affect the swing arm assembly, C-clamps, and fixture have on the plate mode shapes. The relationship between each component are studied and its effect on the plate's dynamic response are determined. The input parameters in the finite element model are changed to correlate with the testing results.

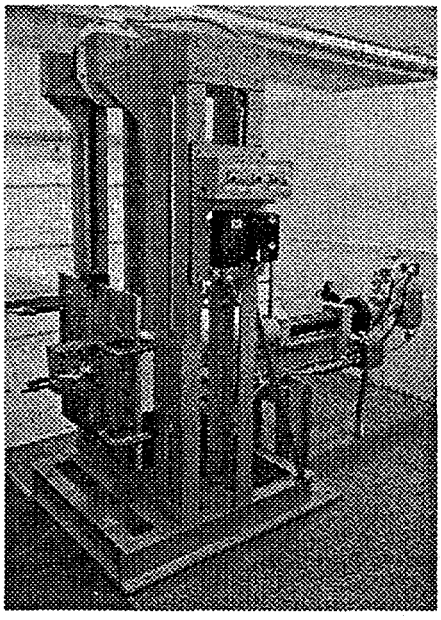

Figure 2. Test apparatus.

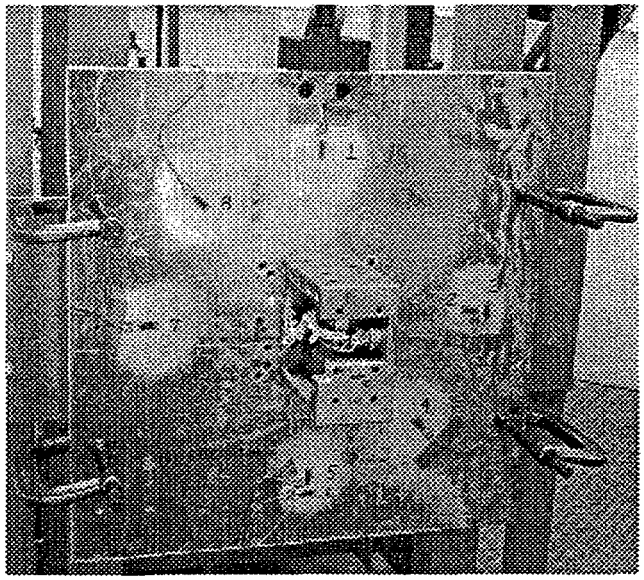

Figure 3. Strain gage orientation.

EXPERIMENTAL PROCEDURE AND ANALYSIS

The experimental procedure is divided into a series of tests. Each test records the strain rate history and acceleration time history for each test configuration. The test matrix is divided into four distinct test configurations. The configurations are: 1) the whole assembly (fixture and C-Clamps); 2) the whole assembly without the C-Clamps; 3) without the fixture but with the C-Clamps; and 4) the free plate. Each data set is reviewed for accuracy and prominent tests are identified.

Each strain gage response is compared to the same gage from a different test in the matrix. Both strain gage intensity and time response are evaluated for errors. After this review, the peak strain response and variation are recorded. The variation in strain ranged from 30-60 microstrain. In terms of stress, this equates to 300-600 pounds per square inch applied to the plate from the projectile. The Fourier transform is used to evaluate the frequency content of each key strain gage response. Each acceleration time history data set is compared to the other acceleration time histories from the test matrix. Both acceleration amplitude and time responses are evaluated for errors. After this review, the key acceleration time histories are plotted. The chosen method to measure shock severity is the shock response spectrum (SRS). The SRS algorithms used to evaluate the acceleration data are taken from the work of Smallwood [8].

ANALYTICAL PROCEDURE

The analytical procedure is divided into a series of modeling steps. The first step creates a geometric model of the plate with the correct dimensions. This task is completed in I-DEAS™ geometry modeling. After geometric modeling is complete a mesh is created of the plate. The mesh size for this model is 0.25 inches. The element type assigned for the plate mesh is a thin shell linear quadrilateral element.

The second step in the analytical procedure is characterize the plate dynamics. This is completed by executing the model using only the initial boundary conditions. The eigenvalues and mode shapes are extracted. The boundary conditions are changed and the model is again executed. The new eigenvalues and mode shapes are compared to the previous run. This iteration process determines how the eigenvalues and mode shapes are affected. The changes in boundary conditions also document if rigid body motion of the plate exists and helps determine the response that produces a 250 Hz resonance. The boundary conditions employed on the finite element model simulate the full contact force of the clevis acting on the plate. The first three eigenvalues and mode shapes are extracted. Rigid body motion of the plate occurs at a frequency of 35 Hz. Asymmetrical bending of the plate occurs at 65 Hz and 166 Hz.

The third step in the analytical procedure adds the swing arm assembly to the plate. Linear brick solid elements are used to model the steel clevis, steel swing arm, and steel mounting block (Fig. 4). The three mechanical components are attached to the plate at the appropriate nodes. This brick element has the desired properties for the impact dynamics and reduces the chance of an instability occurring during program execution. The final swing arm assembly and plate are

connected to the brake shaft. The brake shaft is modeled as a node-to-node rotational spring. The brake pressure is translated to rotational stiffness. This stiffness value is added to the shaft formulation. The spring property is a nonlinear spring. This formulation creates a continuous load on the shaft which simulates a constant brake pressure.

The fourth step in the analytical procedure is to reduce the computational effort and the programmer materials to the plate. This task is accomplished by converting the full plate model to a half plate model. For this transition to be successful, the half plate model should closely display the same mode shapes and resonant frequencies as the previous full plate model. The full model is reduced by the axis of symmetry. Rigid body motion of the plate occurs at 31 Hz. After the reduction is successful, the Delrin-felt programmer materials are attached to the plate (Fig. 5). Isoparametric brick elements are used to model the two programmer materials. The Delrin material is modeled with the Delrin diameter while the felt is modeled with the projectile diameter. The projectile is modeled as a one layer continuous element which simulates the entire length of the projectile. Stiffness and density are adjusted to correlate the energy input into the plate and the restitution response of the projectile. A thin layer of interface elements is also added to the model. These elements are placed between the projectile and the Delrin-felt interface. The characteristic of this element is a four node preface element connected to an eight node Delrin-felt brick element. The interface element attaches to the front face of the Delrin-felt elements. A space is allowed between the projectile and Delrin-felt elements. This space creates an integration point between the two element types. Finite element strain responses are recorded into output files and correlated to the experimental data.

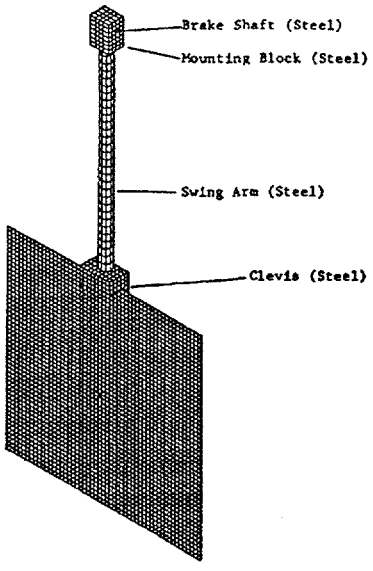

Figure 4. Full plate model.

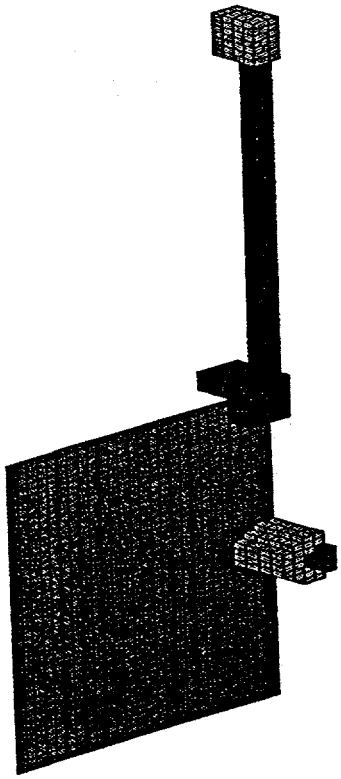

Figure 5. Half plate finite element model.

The final step in the analytical procedure is to model the 5-inch C-Clamp and the fixture; then attach them to the plate. The C-Clamp is modeled and eigenvalues and mode shapes are extracted. To verify the analytical results an accelerometer is bonded to a C-Clamp. Acceleration time history data is collected and analyzed for several projectile impacts. A high speed camera is used to capture the motion of the C-Clamps attached to the plate. The camera recorded the dynamic interaction between the plate and the C-Clamps. This dynamic motion is compared to the experimental and analytical results. The fixture is modeled with solid linear brick elements. This element is chosen because the integration network for strain output is located on the nodes. Computer runs attaching the C-Clamp and fixture to the free plate are conducted. To attach the C-Clamp to the plate two additional inputs are required. The first addition is the equation statement. The equation statement allows an equation to be written representing nodes in the model. Constraints are applied to the nodes where the C-Clamp attaches to the plate. The degrees of freedom are tied together. The displacement in the x direction of the first node minus the displacement in the x direction of the second node must equal zero. If the equation statement is used solely the node can rotate around itself. To eliminate this condition, the Multi-Point Constraint statement is used. Multi-Point Constraint allows constraints to be imposed between either different degrees of freedom on different nodes or the same constraints between the same degrees of freedom on different nodes. To accurately define the model, both sides of the C-Clamp must respond like the two plate nodes.

RESULTS

The initial experiments utilized accelerometers attached at four locations to characterize the plate dynamics. These responses developed a better understanding of the C-Clamp to plate interaction. Figure 6 reveals the response differences of the full assembly with C-Clamp removal. Higher accelerations occur with C-Clamp removal. The biggest change in the accelerometer response is the measured frequency. Higher frequencies exist throughout the acceleration time history with C-Clamp removal. The predominate frequencies from Fourier analysis are 205, 550, 750, and 1500 Hz . The higher frequencies are higher modes shapes of the plate. The removal of the C-Clamps causes a the maximum shock response to shift and occur at a higher peak value.

The strain experiments characterized the dynamic response of the plate. These responses helped develop the correct boundary conditions for the finite element model. The removal of the C-Clamps from the full assembly causes the plate to respond longer (fig. 7 and fig 8.). The predominate frequencies are 90, 154, and 204 Hz. The removal of the C-Clamps does not cause the strain values to increase but shifts the response frequency. The plate ringing is dominate in the lower gages. After the first half cycle impending wave fronts develop. This phenomenon occurs from the reoccurring shock waves rebounding from the edge of the plate. As the distance from the clevis increases, higher frequencies develop in the plate. The removal of the C-Clamps does cause the strain values to decrease in the second half cycle in the lower plate. The decrease in strain is from the inertia properties of the C-Clamps.

For the free plate condition without the C-Clamps attached gage 3 shows that the peak response from the analytical data is greater than the peak response from the experimental data (fig. 9). The peak responses from the analytical and experimental data are similar for gage 3. For the full

assembly plate condition without the C-Clamps, gage 3 shows the peak response from the experimental data is greater than the peak response from the analytical data (fig. 10). With the C-Clamps attached to the full assembly however, the peak response from the experimental data is greater than the analytical data for gage 3.

The results of the finite element test runs are correlated between the strain gage and accelerometer responses. The effect of changing boundary conditions on the plate response are extracted from the models and compared to the experimental results. Strain rate histories are calculated and stored for each test case. The results from the experimental strain gage analysis and acceleration analysis revealed the dynamic characteristics of the plate. The finite element analysis calculated the normal mode dynamics of the free plate and calculated the strain rate histories at the experimental strain locations.

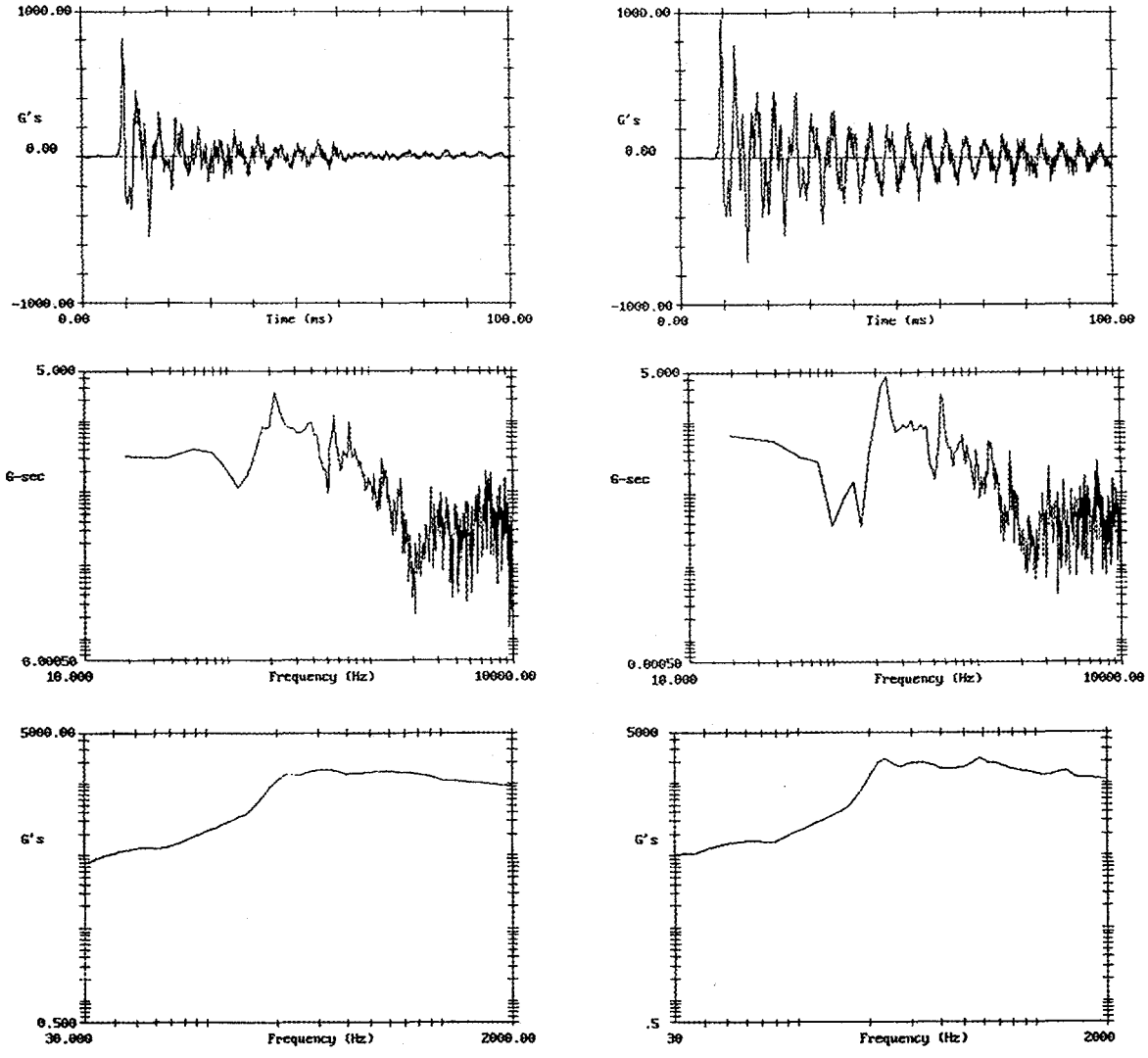

Figure 6. The acceleration time history, Fourier transform and shock response spectrum for the accelerometer located on the fixture. The second column is the response from C-Clamp removal.

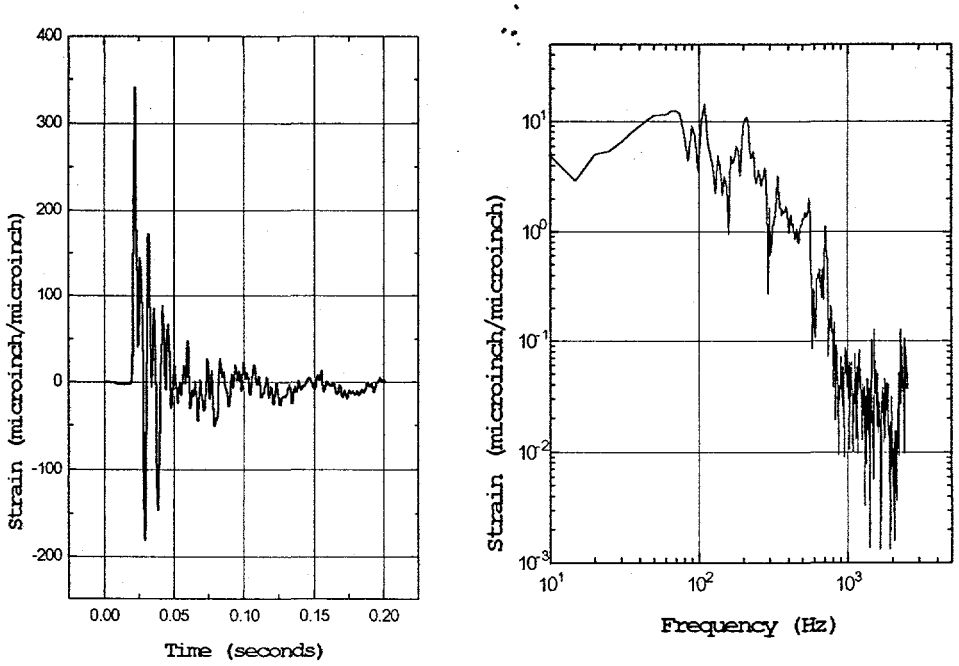

Figure 7. Strain gage #3 response and its Fourier transform for the full plate configuration.

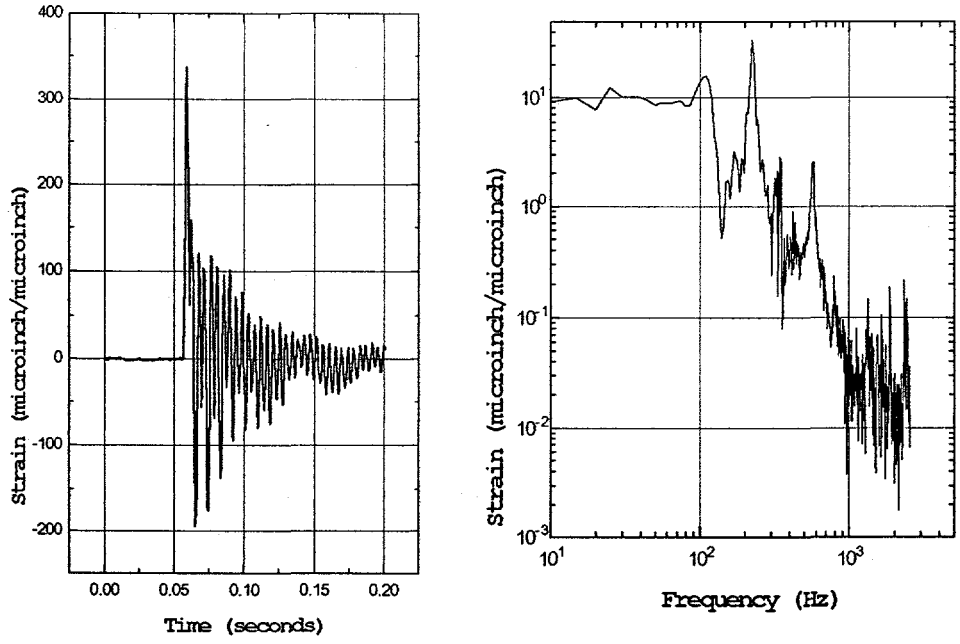

Figure 8. Strain gage #3 response and its Fourier transform with C-Clamp removal.

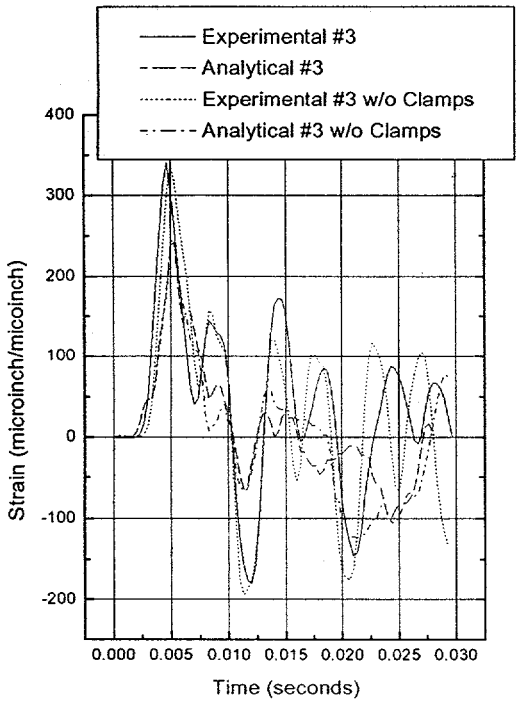

Figure 9. Full assembly configuration.

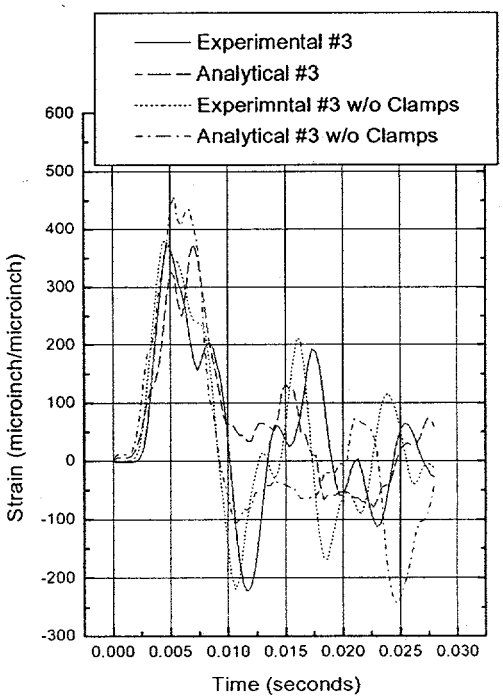

Figure 10. Free plate configuration

CONCLUSIONS

The C-Clamps dampen the high frequency modes in the plate. The resonant frequency of the C-Clamps dissipates some of the energy from the plate. This energy dissipation is caused by the C-Clamps slipping on the plate surface. The C-Clamps also reduce the frequency at the plate resonance and cause the plate to respond to lower out-of-plane frequencies. Higher mode shapes are dominate near the lower plate locations. The C-Clamps add local dampening and inertia loads at the lower plate and cause the plate to respond with larger strain amplitudes.

The distance between the clevis and the accelerometer determines the frequency content. Higher frequencies are predominate at locations away from the clevis. Acceleration values are higher at the center of the plate. The mass at the center of the plate creates more plate deflection and adds lower mode shapes to the plate response. Higher accelerations and smaller damping effects on the plate occur with C-Clamp removal. Larger shock responses at peak values occur with C-clamps removal. The removals of the C-Clamps also cause the maximum shock response to shift.

The calculated peak strain response for gage 3 without the C-Clamps is larger than the peak strain response with the C-Clamps for the free plate condition. The frequency content for the calculated strain are similar. The experimental peak strain gage response did not display this characteristic. The calculated peak strain response for gage 3 without the C-Clamps is similar to the peak strain response with the C-Clamps attached to the full plate assembly. The experimental peak strain gage response displays the same results as the calculated values. Higher frequencies (above 1000 Hz) are reduced when the C-Clamps is attached to the plate.

REFERENCES

1. Bai, Monty and Thatcher, Wesley, "High G Pyrotechnic Shock Simulation Using Metal-to-Metal Impact", Shock & Vibration Symposium, Sept. 1979, No. 49, Part 1, pp. 97-100.

2. Davie, Neil T., "The Controlled Response of Resonating Fixtures Used to Simulate Pyrotechnic Environments", The Shock and Vibration Bulletin, Bulletin 56 Part 3, August 1986, pp. 119-123.

3. Bell, R. Glenn and Zimmerman, Roger M., "Test Component Attachment Effects on Resonate Plate Pyrotechnic Shock Simulation", Institute of Environmental Sciences, Proceedings 1990, pp. 720-724.

4. Bell, R. Glenn and Pott, J., "Understanding the Effects of Damping Systems on Resonant Plates", 7th International Modal Analysis Conference Proceedings, February 1989, pp. 1221-1226.

5. Timoshenko, S. P. and Woinowsky-Krieger S., "Theory of Plates and Shells", Second Ed., McGraw-Hill Book Co., Inc., 1959, pp. 1-54.

6. Leissa, Arthur, W., "Vibration of Plates", Office of Technology Utilization, National Aeronautics and Space Administration, 1969, pp.331-337.

7. Bathe, K. J., "Finite Element Procedures in Engineering Analysis", Prentice-Hall Inc., 1982, pp. 315-319.

8. Smallwood, D. O., "The Shock Response Spectrum at Low Frequencies", Washington D.C. Shock and Vibration Center, Naval Research Laboratory, The Shock and Vibration Bulletin, Vol. 56, Part 1, August 1986, pp. 279-287

BIBLIOGRAPHY

ABAQUS Standard User's Manual II, Version 5.2, Hibbitt, Karlson, and Sorensen, Inc. 1992.

ABAQUS Theory Manual, Version 5.2, Hibbitt, Karlson, and Sorensen, Inc. 1992.

"I-DEAS Finite Element Modeling User's Guide", Structural Dynamics Research Corp., 1990.

D. G. Moore, Masters Defense, "Simulation of Resonant Plate Shock Testing Using Finite Element Analysis", University of Missouri -Columbia, December 1994.